JOURNAL OF GEOPHYSICAL RESEARCH, VOL. 100, NO. B4, PAGES 6367–6381, APRIL 10, 1995

Climate change on the Colorado Plateau of eastern Utah inferred from borehole temperatures

Robert N. Harris and David S. Chapman
Department of Geology and Geophysics, University of Utah, Salt Lake City

Abstract. Temperature profiles from boreholes on the Colorado Plateau of southeastern Utah have been examined for evidence of climate change. Because these boreholes penetrate layered sedimentary rocks with different thermal conductivities, Bullard plots (temperature versus integrated thermal resistance) are used to estimate background heat flow and surface temperature intercepts. Reduced temperatures, which represent departures from a constant heat flow condition, are inverted for a surface ground temperature history at each borehole site using a singular value decomposition algorithm. Singular value cutoffs are selected by analyzing the spectral energy and the standard deviation of the model fit to the data as a function of the number of eigenvalues; solutions are constructed from areas of large spectral energy and a cutoff where additional eigenvalues fail to improve the solution significantly. The solution is parameterized in terms of 13 time steps increasing in duration and going back 400 years. Eight of nine borehole sites indicate between 0.4 and 0.8°C (±0.2°C) warming over the past 200 years with some evidence for accelerated warming in this century; one borehole indicates local cooling over the same time period. The amplitude of the warming inferred from borehole temperatures is less than that deduced from analysis of 100-year surface air temperature records at four of the five weather stations surrounding the borehole sites.

Introduction

The strongest evidence for recent and widespread climatic warming comes from analysis of surface air temperature (SAT) measurements [*Wigley et al.*, 1985; *Ellsaesser et al.*, 1986; *Hansen and Lebedeff*, 1987; *Jones and Briffa*, 1992; *Briffa and Jones*, 1993]. Global analysis of SAT trends shows an increase of 0.5-0.7°C in the last 100 years but also shows spatial variability as a function of latitude [*Hansen and Lebedeff*, 1987]. Some high-latitude regions exhibit 3-5°C of warming, while midlatitudes show less warming; some equatorial regions show no warming or even show cooling. Unfortunately, for most areas, coverage of SAT data is limited in space (few stations) and in time (this century).

Changes in temperature at the Earth's surface, however, propagate slowly downward into the Earth and perturb the subsurface temperature field. Due to the relatively low thermal diffusivity of rock (1×10^{-6} m^2 s^{-1}), temperature perturbations in the uppermost 300 m of the Earth's crust reflect surface temperature conditions over the past few hundred years. These subsurface temperature perturbations therefore can be used to reconstruct past surface ground temperature trends not only for this century but also for the time immediately preceding installation of weather stations, a period of time that is critical to climate change studies.

Analyses of borehole temperature logs both complement and extend the meteorological archive of climate change data. Surface ground temperature changes inferred from geothermal data include 2-4°C of warming in northern Alaska [*Lachenbruch and Marshall*, 1986; *Lachenbruch et al.*, 1988], 1-2°C of warming in central and eastern Canada [*Nielson and Beck*, 1989; *Jessop*, 1990; *Beltrami and Mareschal*, 1991, 1992; *Wang and Lewis*, 1992], 1.5°C warming in France [*Mareschal and Vasseur* 1992], variable warming between 0 and 2°C for the northern U.S. plains [*Gosnold and Bauer*, 1990], warming of about 2°C in the southern U.S. plains [*Deming and Borel*, 1993] and an average of 0.6°C warming in the northern Basin and Range of Utah [*Chisholm and Chapman*, 1992; *Chapman et al.*, 1992]. While the timing of warming is loosely constrained, these studies indicate that ground warming has occurred over the past 100 to 150 years. In some cases [*Chisholm and Chapman*, 1992; *Chapman et al.*, 1992] long-term surface temperature changes inferred from borehole temperatures are significantly less than changes computed from 100-year or shorter records of air temperatures at nearby weather stations.

It is important to extend studies of climate change inferred from borehole temperatures to a variety of climatic zones and geologic settings to track past climatic events spatially and temporally. Most previous studies of borehole temperature logs used to infer temperature change at the Earth's surface use data from permafrost regions or in crystalline rock. This paper extends the study of inferring climate change from borehole temperatures both to a new geographic and climatic region, the Colorado Plateau of southeastern Utah, and to a geological setting of layered sedimentary rocks where thermal conductivity variations must be included explicitly in the analysis.

Geothermal Data and Analysis

Temperature-depth profiles used in this study come from nine sites (Figure 1) in the Colorado Plateau of southeastern Utah within the San Rafael Desert (SRD) and the San Rafael

Paper number 94JB02165.
0148-0227/95/94JB-02165$05.00

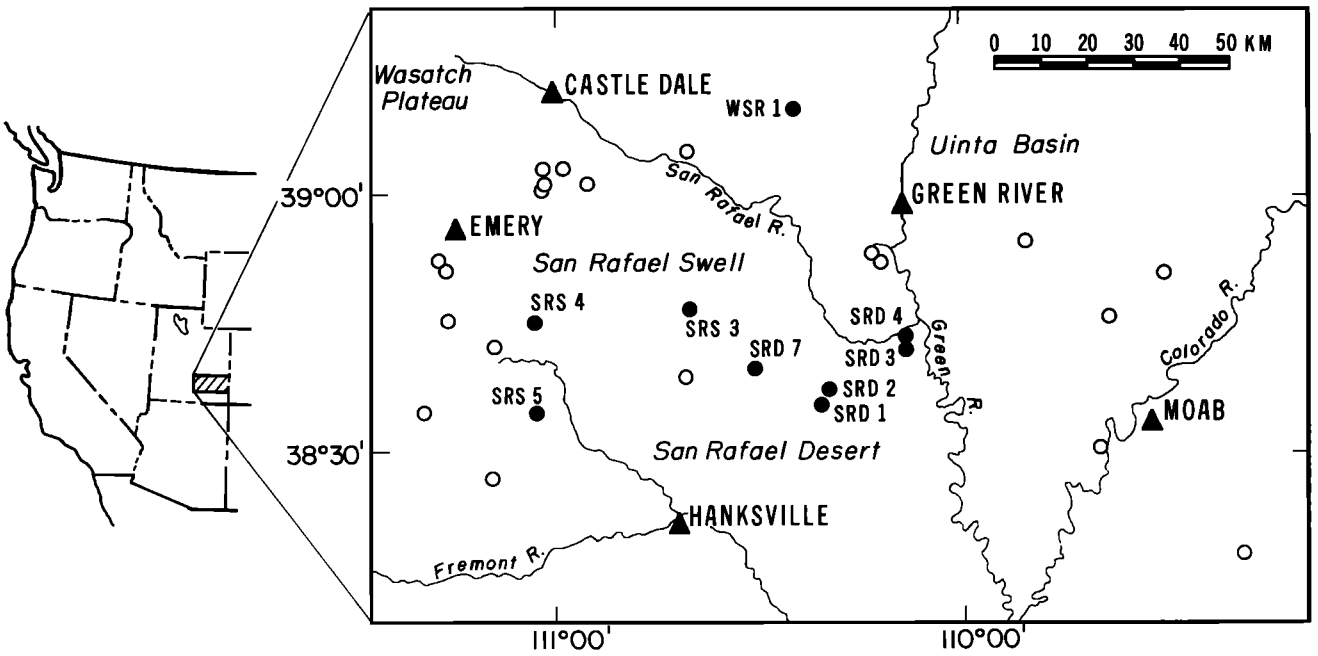

Figure 1. Index map showing borehole sites (circles) and meteorological stations (triangles) for part of the Colorado Plateau of southeastern Utah. Borehole sites selected for this study are shown as solid circles.

Swell (SRS) physiographic subprovinces. The boreholes were drilled by mining companies between 1976 and 1980. These temperature logs form a subset of a larger data set originally used in a regional heat flow study [*Bodell and Chapman*, 1982]. Sites used in this climate reconstruction study were selected using the following criteria: (1) borehole temperature logs extend to a depth of at least 300 m, (2) temperature logs show no obvious sign of groundwater flow, and (3) temperature logs show a consistent thermal gradient through individual sedimentary units. These criteria eliminated 19 sites (also shown in Figure 1) that had been used for heat flow determinations.

Temperature-depth measurements were made using a thermistor probe, four-conductor cable, and a digital ohm meter in stop and go mode. All thermistors used were calibrated in the laboratory against a Hewlett Packard 2804A quartz thermometer. The precision and accuracy of the measurements are estimated to be better than 0.01 K and 0.1 K, respectively [*Bodell and Chapman*, 1982]. Details of instrumentation and measurement procedure are reported by *Chapman* [1976] and *Chapman et al.* [1981].

Temperature-depth measurements for the nine borehole sites are shown in Figure 2, in which the profiles are plotted against relative temperature to avoid overlap. Boreholes selected in the San Rafael Desert are between 300 m and 450 m deep and in the San Rafael Swell are between 500 m and 600 m deep. Boundaries between sedimentary formations are marked on the temperature-depth profiles and formation abbreviations are given in Table 1. Because these temperature measurements were made for a regional heat flow survey where the focus was on temperature gradients in the deepest portion of each borehole rather than fine-scale temperature perturbations near the surface, the measurement density is coarse. In the deeper portions of the boreholes the measurement spacing is usually 5 m, but in the shallow part of the boreholes where the temperatures are most sensitive to a changing surface condition, the measurement spacing increases from 5 to 10 m for most boreholes (SRD-1, SRD-3, SRD-4, and SRS-3); in SRD-2 the measurement spacing is 25 m (Figure 2). Previous studies, however, have indicated that the temporal resolution of temperature histories is only slightly sensitive to the vertical spacing of measurements [*Clow*, 1992; *Mareschal and Beltrami*, 1992; *Beltrami and Mareschal*, 1994].

For a homogeneous, isotropic medium having no internal heat sources and bounded top and bottom by planar constant temperature surfaces, with the lower surface hotter than the upper surface, temperature increases linearly with depth. The temperature gradient is a function of heat flow and the thermal conductivity of the medium. The Earth's crust, however, seldom approaches such a thermal condition. Perturbations to this ideal thermal state are caused by various mechanisms including contrasts in thermal conductivity, heat production, surface elevation effects, surface temperature variations, erosion or burial, groundwater flow, and changing surface temperature with time [*Jaeger*, 1965; *Beck*, 1982; *Chisholm and Chapman*, 1992, appendix A].

The largest nonclimatic source of temperature perturbation in our Colorado Plateau data set (Figure 2) is thermal conductivity contrasts manifested as changes in thermal gradient for different sedimentary formations. Good examples of gradient breaks caused by conductivity contrasts are found in SRD-1, SRS-4, and WSR-1 across the Carmel-Navajo horizon and in SRD-4, SRD-7, and SRS-5 across the Wingate-Chinle horizon, also pointed out by *Bodell and Chapman* [1982]. The temperature-depth variation attributable to thermal conductivity differences can be isolated, however, by computing temperature residuals for a condition of constant heat flow rather than a constant gradient as is done with homogenous rock. We use the *Bullard* [1939] method, which combines measured temperatures and thermal conductivities for a stratified medium to estimate background heat flow q_o and surface temperature intercept T_o. In this method,

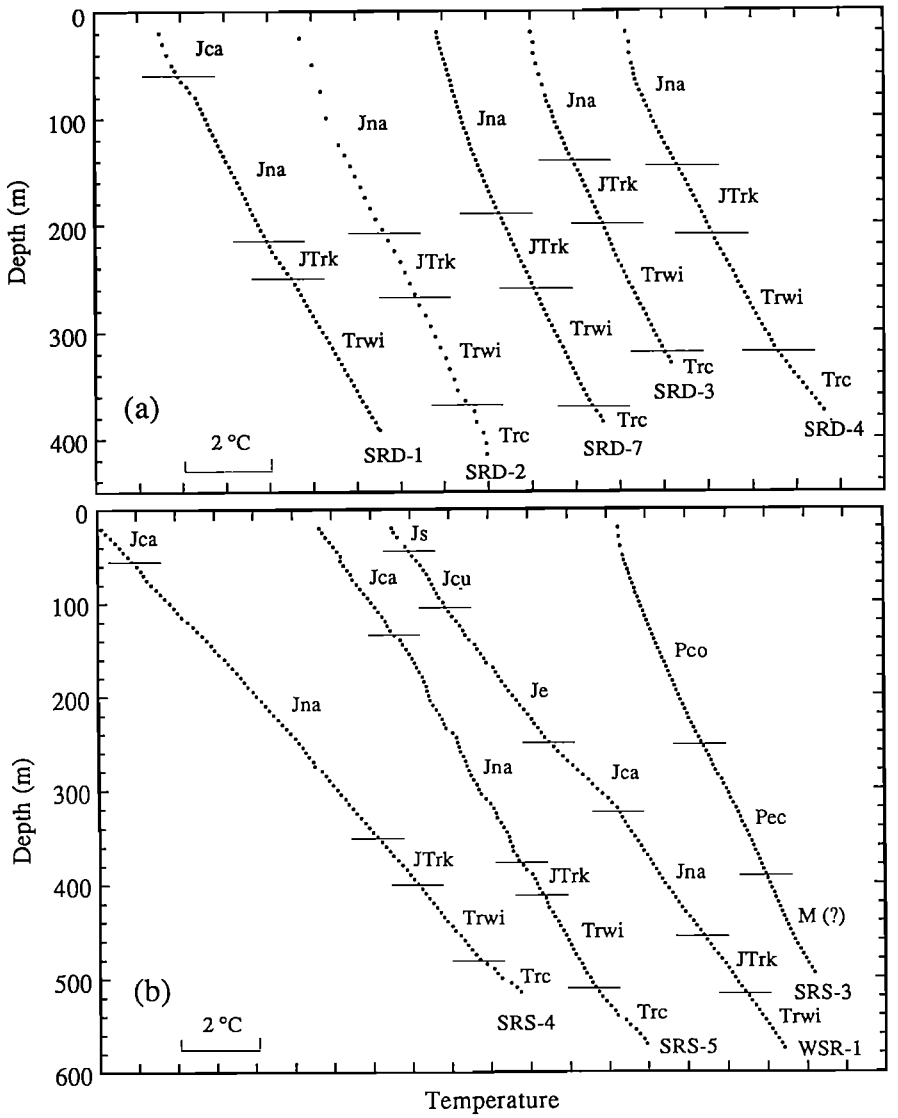

Figure 2. Temperature-depth profiles for (a) San Rafael Desert (SRD) and (b) San Rafael Swell (SRS and WSR) sites. Site locations are shown in Figure 1. Relative temperatures are used to avoid overlap. Lithology symbols are given in Table 1. Note the temperature gradient breaks associated with the sedimentary formation boundaries (denoted as horizontal lines). Formation abbreviations are identified in Table 1.

subsurface temperatures may be expressed as

$$T(z) = T_o + q_o \sum_{i=1}^{N} \frac{\Delta z_i}{k(z)_i} \quad (1)$$

where $k(z)_i$ is the thermal conductivity measured over the ith depth interval Δz_i and the summation is performed over N depth intervals from the surface to the depth of interest z. In practice, q_o and T_o are estimated by plotting $T(z)$ against summed thermal resistance $\Sigma(\Delta z_i/k(z)_i)$. The key to this method is to have well-constrained thermal conductivities for each unit. Thermal conductivity measurements made on 118 solid rock discs sampled from the relevant Colorado Plateau sedimentary sections at our sites are summarized in Table 1 (see also *Bodell and Chapman* [1982, Table 2]).

In our first attempt to remove breaks in thermal gradients associated with formation boundaries we used the measured conductivities (Table 1) to construct Bullard plots. Analysis of these plots, however, indicated that the effect of contrasting thermal conductivities is only partially removed. Note that the standard deviation of thermal conductivity measurements in many formations is between 0.3 and 0.7 W m^{-1} K^{-1}. Here we explore whether a better estimate of in situ conductivity for some of these formations can be obtained by using the ensemble of boreholes and solving for thermal conductivity assuming a constant vertical heat flow condition in each borehole below 100 m depth, where the climate signal is attenuated. Additionally, we adjust conductivities only for formations that occur in multiple boreholes. These formations are Carmel, Navajo, Kayenta, Wingate, and Chinle (Table 1).

Our goal is to find a single adjusted conductivity for each formation which gives the best realization of a constant heat flow condition below 100 m. The condition of constant heat flow at depth is expressed as

$$k_{n,i} = \frac{\Gamma_{n,o}}{\Gamma_{n,i}} k_{n,o}, \quad (2)$$

Table 1. Formations and Thermal Conductivities

Period	Formation	Symbol	Lithology	N	k_{pr} W m^{-1} K^{-1}	(s.d.)	SRD k_a W m^{-1} K^{-1}	SRS k_a W m^{-1} K^{-1}	ϕ %	(s.d.) %
Jurassic	Summerville	Js	Sltst	1	4.10	(---)	---	---	1.2	(---)
	Curtis	Jcu	Cgl	4	3.96	(0.51)	---	---	1.6	(0.3)
	Entrada	Je	Sltst-Ss	19	3.43	(0.67)	---	---	6.4	(2.4)
	Carmel	Jca	Mdst-Ss	17	2.75	(0.58)	---	2.91	2.9	(2.7)
	Navajo	Jna	silty Ss-Ss	24	4.18	(0.72)	4.09	4.18	11.8	(2.6)
Triassic	Kayenta	JTrk	silty Ss-Ss	14	4.20	(0.54)	3.96	3.86	12.5	(3.4)
	Wingate	Trwi	Ss	17	3.86	(0.37)	3.86	4.17	14.1	(4.8)
	Chinle	Trc	Sltst-Cngl	8	4.11	(1.30)	4.78	2.54	6.6	(3.9)
Permian	Coconino	Pco	Ss	5	5.01	(0.36)	---	---	16.2	(1.5)
	Elephant Canyon	Pec	Dol-Ss	7	4.35	(0.63)	---	---	8.8	(3.4)
Mississippian	Redwall	Mr(?)	Dol	2	4.82	(0.18)	---	---	1.2	(0.5)

N is number of samples; k_{pr} is porous measured rock thermal conductivity for solid rock discs as reported by *Bodell and Chapman* [1982]; k_a is adjusted thermal conductivity for San Rafael Desert (SRD) and San Rafael Swell (SRS); and ϕ is the effective rock porosity. Lithologies are Slst, siltstone; Cngl, conglomerate; Ss, sandstone; Mdst, mudstone, and Dol, dolomite.

where the product ($\Gamma_{n,i} \times k_{n,i}$) represents the heat flow of the ith formation in the nth borehole, $k_{n,o}$ represents the measured conductivity, and $\Gamma_{n,o}$ represents the estimated thermal gradient for a reference formation in that borehole. A reference formation is selected and conductivities of the other formations are adjusted to satisfy a constant heat flow condition. To obtain a single conductivity for each formation from an ensemble of boreholes, we select the best set of conductivities (equivalent to finding the best reference formation) as those which give (1) the best realization of the constant heat flow condition (i.e., minimum temperature residual to a straight line on a Bullard plot), (2) the most consistent results in terms of adjustments to measured conductivities (i.e., minimum standard deviation of conductivities for each formation across several boreholes), and (3) minimized adjustment to the measured conductivities (i.e., minimize the difference between the measured conductivities and the adjusted conductivities weighted by formation thickness). Conceptually, we expect the reference formation to have both a well-constrained measured thermal conductivity and estimated thermal gradient. These expectations translate into a thick, laterally homogenous formation where measured conductivities are most representative of the true conductivity and for the formation to be deep in the borehole below surface-related temperature perturbations.

We first combined all of the boreholes, but we found that the adjustments to the measured conductivities were more consistent if we separated the SRD data from the SRS data. This may be indicative of a facies change between the two subprovinces manifested as a lateral thermal conductivity change. Results indicate that for the SRD data the conductivities are best referenced to the Wingate formation, a thick laterally homogenous sandstone found below 200 m in the SRD boreholes (Figure 2). Adjusted conductivities for the SRS data are referenced to the Navajo Sandstone. The Navajo is also laterally homogenous and occurs from about 100 to 400 m below the surface in SRS boreholes (Figure 2). In both of these cases we were able to satisfy simultaneously the three criteria listed above.

Adjusted conductivities are given in Table 1. In general, the differences between measured and preferred conductivities are small. Adjustments made for the Carmel, Navajo, Kayenta, and Wingate formations average 4.1% and do not exceed 8%. The large variation of conductivity for the Chinle formation may result from a facies change between sites as the lithological variation within the formation is also large.

Bullard plots of temperature versus summed thermal resistance constructed using the conductivities listed in Table 1 are illustrated in Figure 3. Formation boundaries are marked on the Bullard plots and illustrate that we are largely successful at removing temperature variations due to conductivity contrasts across formation contacts. However, one example of a formation where no single conductivity gives a constant heat flow condition is the Chinle Formation. This formation is highly heterogeneous; it consists of sand and shale members, two lithologies with very different thermal conductivities. Because this formation has such a variable conductivity, occurs at the bottom of the boreholes, and is thin, we have excluded it from the subsequent analysis.

To investigate temperature perturbations in the borehole profiles that might be caused by climate change, we use reduced temperatures, $T_r(z)$, defined as

$$T_r(z) = T_{obs}(z) - \left(T_o + q_o \sum_{i=1}^{N} \frac{\Delta z_i}{k(z)_i} \right). \quad (3)$$

Reduced temperatures represent departures from a constant heat flow condition. The reducing parameters T_o and q_o for each borehole were found by linear regression on the Bullard plots below the depth where the climate signal becomes negligible. To determine this depth, we plotted rms misfit between the observed temperatures and the best fitting constant heat flow condition as a function of the depth to the start of fit. The SRD Bullard plot data are approximately linear (i.e., constant heat flow) below 150 m, and the SRS data are approximately linear below 200 m. With these respective depth limits, surface intercept temperatures and background heat flow values for (3) were computed; the results are given for our nine boreholes in Table 2. The heat flow values agree well with those given in Table 3 of *Bodell and Chapman*

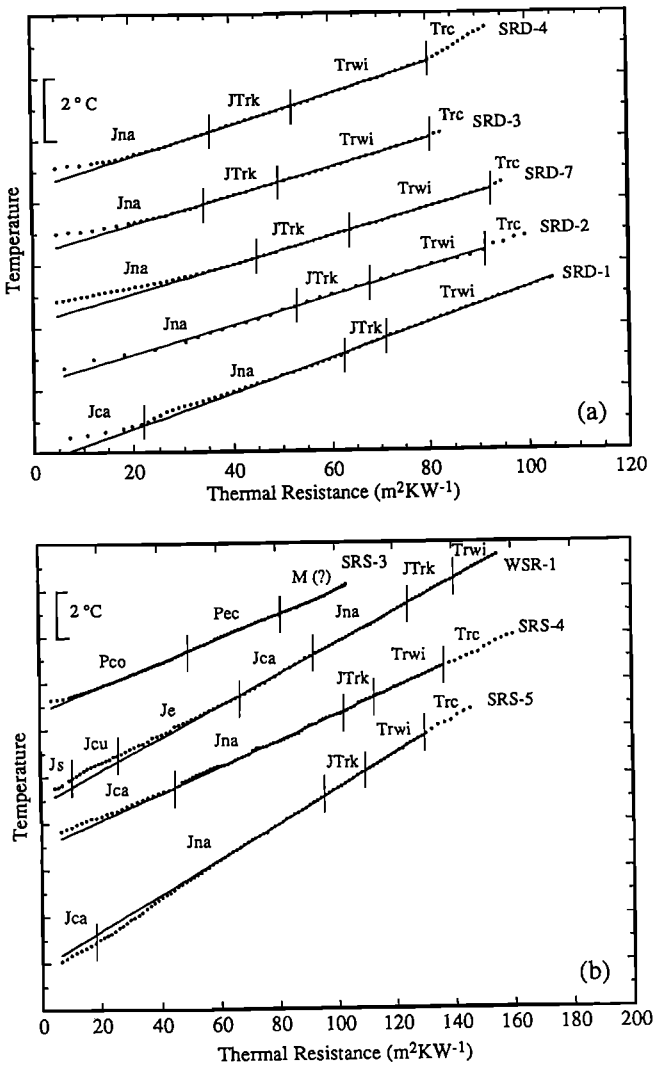

Figure 3. Bullard plots of temperature versus summed thermal resistance for (a) San Rafael Desert (SRD) and (b) San Rafael Swell (SRS and WSR) sites. Relative temperatures are used to avoid overlap. Dots show data, and line shows best fit of data below the climatically perturbed region. Estimates of surface intercept temperatures T_o and heat flow q_o (i.e., slope of the Bullard plot) are given in Table 2. The Chinle Formation is not used in computing heat flow. Formation abbreviations are identified in Table 1.

[1982] computed using measured conductivities and the entire depth of the borehole.

Reduced temperatures for each borehole are shown in Figure 4. These plots have an expanded temperature scale that accentuates departures from the constant heat flow condition. At eight of the nine sites, reduced temperatures near the surface are systematically positive, having an amplitude of 0.2°C to 0.5°C and a depth extent of between 100 and 200 m. Borehole SRS-5, however, shows a negative departure at depth that is maximum at a depth of 70 m. Below 200 m the average reduced temperature for the collection of sites is zero. In the deeper portions of the boreholes, longer-wavelength (> 20 m) departures from zero-reduced temperature are probably caused by small thermal conductivity deviations from values used with the Bullard plot reduction. Short-wavelength scatter may be caused by measurement imprecision or local thermal perturbations in the borehole. Average rms reduced temperature below 200 m in this data set is 0.024 K.

We believe that the reduced temperature anomalies in Figure 4 are caused by gradual warming of the surface over the last 100 to 200 years. Alternative explanations for the reduced temperature anomalies are quantitatively examined and discounted in a later section after exploring the nature of possible transient warming and its comparison with meteorological data from the same region.

The Inverse Problem

The inversion problem consists of determining the surface ground temperature history from reduced temperature data. For a homogenous, source-free half-space where heat is transferred by conduction, reduced temperatures satisfy the one-dimensional heat diffusion equation

$$\frac{\partial^2 T_r(z,t)}{\partial z^2} = \frac{1}{\alpha}\frac{\partial T_r(z,t)}{\partial t}, \tag{4}$$

where the Earth's surface is at $z = 0$, z is positive down, and α is the thermal diffusivity (1×10^{-6} m^2 s^{-1}). Although thermal conductivity is variable, using reduced temperatures defined by (3) effectively removes this complication. Further, since thermal diffusivity variations between different rock types are an order of magnitude less than thermal conductivity variations, we can safely assume a constant diffusivity medium in our analysis [*Somerton*, 1992]. Surface ground temperature histories are parameterized in terms of N individual step changes in surface temperature of amplitude ΔT_i and time prior to the borehole temperature measurement, t_i. This parameterization leads to a solution of the form [*Birch*, 1948; *Carslaw and Jaeger*, 1959],

$$T_r(z) = \sum_{i=1}^{N} \Delta T_i \operatorname{erfc}\left\{\frac{z}{\sqrt{4\alpha t_i}}\right\}, \tag{5}$$

where erfc is the complimentary error function. The forward problem may be expressed in matrix notation as

$$\mathbf{Gm} = \mathbf{d}, \tag{6}$$

where the data $\mathbf{d}$ are a function of the data kernel $\mathbf{G}$ and

Table 2. Site and Bullard Plot Data

Site	Date Logged	q_o, mW m^{-2}	T_o, °C
	San Rafael Desert		
SRD-1	Aug. 31, 1979	56	13.6
SRD-2	Nov. 19 1976	46	15.2
SRD-3	Sept. 12, 1979	45	15.3
SRD-4	Sept. 12, 1979	49	15.2
SRD-7	April 20, 1980	45	13.1
	San Rafael Swell		
SRS-3	Aug. 30, 1979	51	10.7
SRS-4	Sept. 12, 1979	56	12.0
SRS-5	Sept. 21, 1979	75	11.9
WSR-1	April 19, 1980	68	12.8

q_o is heat flow, and T_o is the surface intercept.

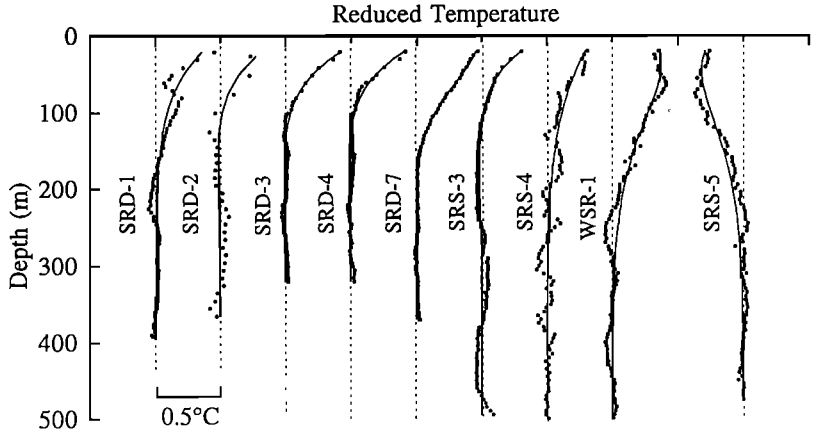

Figure 4. Reduced temperature profiles for a condition of constant vertical heat flow. The dashed line shows 0°C reduced temperature for each site. Reducing parameters T_o and heat flow q_o are given in Table 2. Note the expanded temperature scale. The solid line shows the predicted model from the preferred surface ground temperature history.

parameters **m**. This parameterization leads to a well-conditioned data kernel but has the drawback of amplifying the noise in the reduced temperatures through differencing. We use a time varying interval, giving a fine time spacing in the recent past where the inversion is more sensitive, and we increase the duration of time steps in the past, which helps to stabilize the solution [*Mareschal and Vasseur*, 1992].

Singular value decomposition (SVD) is used to find the solution vector **m** because of the insight offered between model resolution and parameter variance. This technique attenuates instabilities in the solution by nulling small singular values. SVD as an inversion technique is described elsewhere [e.g., *Lanczos*, 1961; *Jackson*, 1972; *Phillips*, 1974; *Lines and Treitel*, 1984] and has been used to determine ground temperature histories [*Mareschal and Beltrami*, 1992; *Beltrami and Mareschal*, 1994], so only the salient points will be developed here. The data kernel **G** is factored as

$$\mathbf{G} = \mathbf{U}\Lambda\mathbf{V}^T, \tag{7}$$

where **U** is the matrix of eigenvectors spanning the data space, **V** is the matrix of eigenvectors spanning the model space, and Λ contains the eigenvalues λ, which are ordered from largest to smallest, and maps the data space into the model space. The generalized inverse is given as [*Lanczos*, 1961]

$$\mathbf{G}^\dagger = \mathbf{V}\Lambda^{-1}\mathbf{U}^T. \tag{8}$$

Eigenvalues near zero lead to instabilities in the solution. Criteria chosen for selecting the number of nonzero eigenvalues, p, used to construct the solution include the fit of the model to the data, expressed as the standard deviation of the data fit,

$$\delta_d = \|\boldsymbol{d} - \boldsymbol{Gm}\|, \tag{9}$$

and the variance of the first model parameter $\sigma^2_{\Delta T1}$,

$$\sigma^2_{\Delta T1} = \sum_{r=1}^{p} \frac{V_{r1}}{\lambda_r^2}, \tag{10}$$

where it is understood that the standard deviation increases for higher-order coefficients so that $\sigma^2_{\Delta T1}$ represents a minimum variance. By using these two criteria to determine p one can optimize the data fit while minimizing the model variance.

A measure of how individual data eigenvectors contribute to the fit of the data is given by the spectrum of the data in the space defined by the data eigenvectors:

$$\psi_n^2 = (\mathbf{U}_p)^2. \tag{11}$$

Eigenvectors associated with relatively little spectral energy and small eigenvalues contribute little to the data misfit compared to their contribution to the uncertainty in the model. As an additional constraint we also looked at the condition number of each data kernel as a function of p. The condition number measures stability of data kernels and represents the sensitivity to which relative errors in the data affect relative errors in the estimates of model parameters. The condition number is given as (λ_1/λ_p).

We illustrate the process of picking the number of nonzero eigenvalues with an example from site SRD-3. Figures 5a and 5b show the diagnostic parameters as a function of the eigenvalue cutoff, p. These plots are representative of the entire data set. The condition number for the data kernel becomes very ill-conditioned for $p > 8$, so only the first eight eigenvalues are plotted. Although the eigenvalues and condition number show no sharp break, the fit of the model to the data, δ_d, fails to decrease significantly beyond $p = 2$ (Figure 5b). Furthermore the spectral energy, Ψ, shows that the first two eigenvalues contribute most significantly to the solution. Together, these plots indicate that the solution corresponding to $p = 2$ should be selected and that solutions corresponding to $p > 2$ represent perturbations to the $p = 2$ solution that are insensitive to the data. Figure 5c shows the surface ground temperature solutions for SRD-3 corresponding to p from 1 through 4. The preferred solution, using $p = 2$, is shown as a solid line. The solution corresponding to $p = 3$ is similar to the $p = 2$ solution, as reflected by the small power in Ψ at $p = 3$ (Figure 5a); the solution corresponding to $p = 4$ shows the effect of incorporating higher frequencies by retaining more eigenvalues. We attribute the high magnitude of the singular values to the instability of the problem and the parameterization which amplifies noise. The low number of

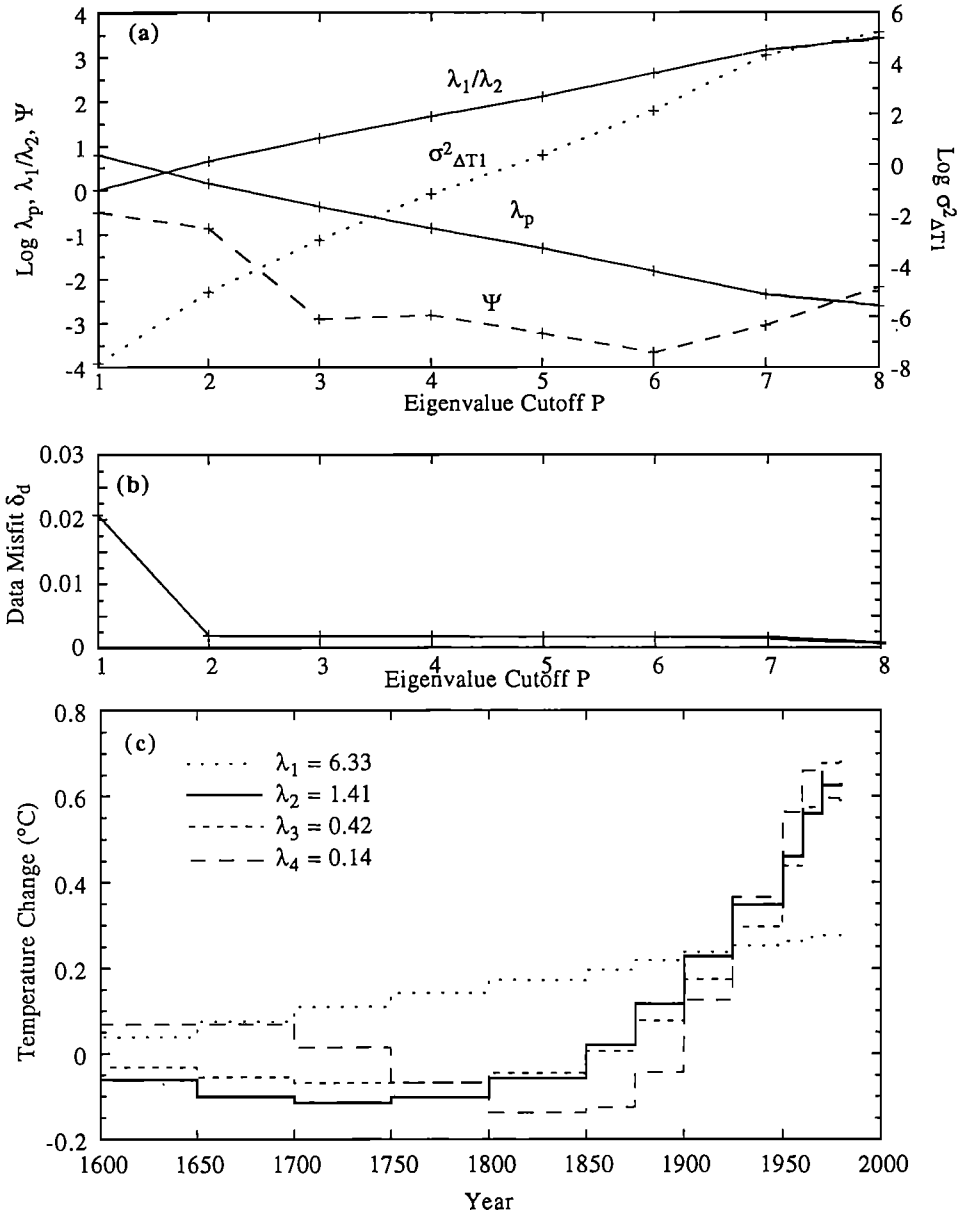

Figure 5. (a) Diagnostic inversion parameters as a function of eigenvalue cutoff p for site SRD-3. Parameters include the eigenvalue (λ_p), condition number (λ_1/λ_p), the variance of model element 1 ($\sigma^2_{\Delta T1}$), and the spectrum of U (Ψ). (b) Standard deviation of the fit to the data (δ_d). (c) Surface ground temperature histories for site SRD-3 as function of eigenvalue cutoff. The model corresponding to λ_2 is the preferred solution.

eigenvalues in the preferred model increases the robustness of the model and approximates a ramp solution.

Plots of the criteria functions for the other borehole reduced temperatures indicate that p = 2 gives the preferred solution with the exception of one site; criteria plots for SRD-7 indicate the preferred solution corresponds to p = 3. Figure 6 shows the preferred solution (solid line) bracketed by the solution corresponding to the next highest (dashed line) and next lowest eigenvalue (dotted line). Figure 4 shows the model predictions superimposed on the reduced temperature plots. This figure shows that we are fitting the broad trends of the data without fitting high-frequency variations which we attribute to nonclimatic perturbations. Most of the preferred solutions (Figure 6) are quite similar, showing 0.6 to 0.8°C warming; significant change begins around 1800 A.D. There is a slight suggestion of an onset of warming as early as 1700 for SRD-1, SRD-7, and SRS-4. The more detailed solution (p = 3) justified for SRD-7 yields an accelerated warming from 1800 to 1950 with subsequent cooling of 0.3°C to the present; the solution for p = 2 conforms more closely to solutions at neighboring sites with equivalent resolution, and the solution corresponding to p = 4 is not perceptably different from the p = 3 solution. The borehole temperature profile at one site, SRS-5, yields cooling of 0.4°C between 1600 and 1900 followed by 0.3°C warming to the present. We have no simple explanation for this divergent pattern in the data set, although the study of *Chisholm and Chapman* [1992] found similar variations between sites in northwestern Utah. Inspection of

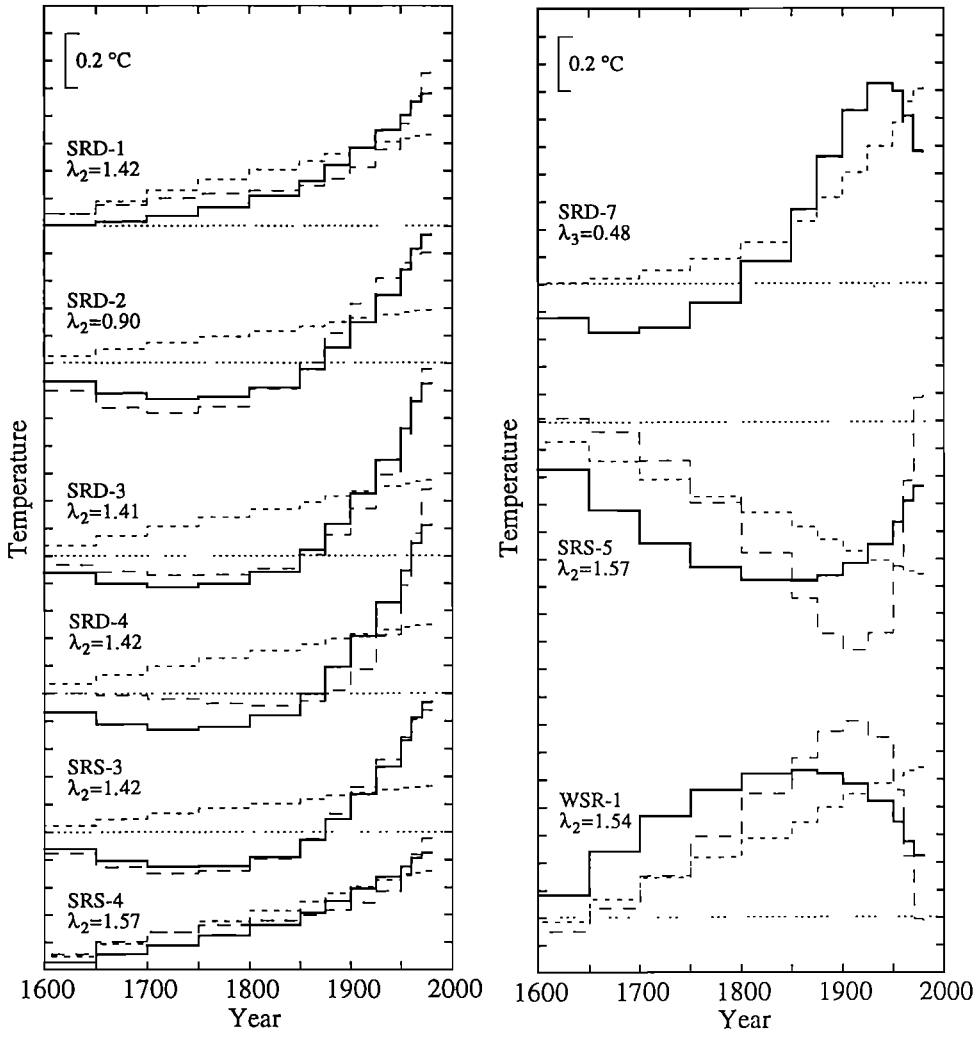

Figure 6. Surface ground temperature histories for all borehole sites. In each case the preferred solution is shown as a heavy line and is bracketed by the model corresponding to the next highest (dashed line) and lowest eigenvalue (dotted line). The eigenvalue cutoff and value for the preferred model is given. Except for SRS-5 and WSR-1 the surface ground temperatures are quite consistent, showing warming from 0.6°C to 0.8°C over about the past 150 years.

air temperature data from weather stations in Utah also yields comparable amplitude temperature variation between sites [*Chisholm and Chapman*, 1992].

Meteorological Data

We have compiled mean annual SAT records from five meteorological stations which surround the boreholes (see Figure 1). Four of the stations (Castle Dale, Emery, Green River, and Moab) are located in a steppe climatic zone, and one station (Hanksville) is in a desert climatic zone (U.S. Weather Bureau). Annual means are computed from monthly means which in turn are computed from daily minimum and maximum temperatures. Daily temperatures are measured 1.5 m above ground surface.

This data set unfortunately suffers from the common weather station problems of incompleteness and location changes. Figure 7a illustrates data gaps and station relocations for these meteorological stations. About 20% of the annual means are missing from the time series (Table 3), and only Castle Dale and Emery have not been moved. Commonly, gaps in mean annual SAT data are filled in by calculating an average offset between a station with missing data and a nearby station, and then using the data from the nearby station, with an appropriate offset, to fill the gap. Station location changes are remedied in a similar manner; an average offset between the station in question and a stable station is calculated before and after the move. The record before or after the move (which ever is shorter) is then adjusted by the appropriate offset. Both of these calculations assume that stations near each other are well correlated. *Hansen and Lebedeff* [1987] demonstrate that the average correlation coefficient for annual temperature residuals between stations is greater than 0.5 for stations that are within 1200 km of each other, although there is much scatter in the data. Recently, *Chisholm and Chapman* [1992] repeated the calculation for seven meteorological stations in western Utah. They find that for stations within 500 km of each other the correlation coefficients range from 0.8 to 0.2. These five stations in the San Rafael Desert and San Rafael Swell are within 200 km of each other.

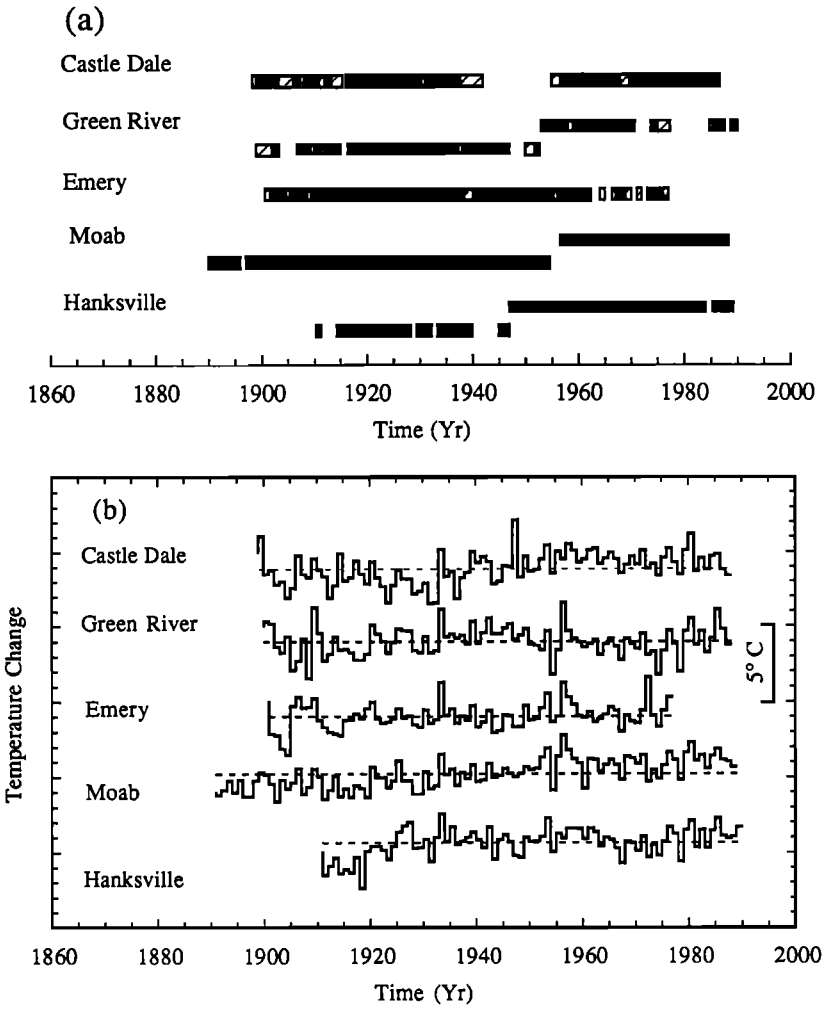

Figure 7. (a) Coverage of meteorological temperature data. Solid bars show times when 12 months of data are present for that year; hatched bars indicate that less than 12 but more than 8 months of data are present; gaps indicate that less than 8 months of data are present. Station location changes are also depicted by shifts in the bar. (b) Surface air temperature data for the meteorological stations shown in Figure 1. Relative temperatures are used to avoid overlap. Average mean annual temperature for each record is given in Table 3.

Before filling in gaps and adjusting for station moves, we checked the correlation of these five stations and found that the correlation coefficient varied between 0.6 and 0.4. In spite of the low correlation coefficients, data gaps and station relocations are remedied as described above. The completed time series are shown in Figure 7b. Long-wavelength features of each SAT time series are modestly correlated, and individual features such as the distinct trough and peak around 1930 appear on multiple records. Linear regression of the five respective SAT time series yields an average temperature increase of 1.34°C per century, but individual stations range from +0.12 to +2.26°C/century (Table 3). Because linear regression of these time series is an oversimplification of the observed patterns we do not put too much weight on the these

Table 3. Calculated Ramp Change in Surface Air Temperature Data by Linear Regression

Station	Span Dates	Number of Years	Number of Years Missing	% Missing	T_{avg} °C	$\Delta T/\Delta t$ °C/100 yrs
Castle Dale	1900-1990	90	32	36	8.0	+1.6
Green River	1900-1990	90	32	36	11.3	+0.1
Emery	1901-1977	77	17	22	7.8	+1.0
Hanksville	1911-1990	79	12	15	11.5	+1.7
Moab	1891-1989	98	3	3	13.0	+2.3

results except to point to the consistency of the results which show warming at all stations. What is unclear however, is whether the warming this century represents a progressive departure from cooler surface temperatures in the past centuries, or whether this temperature increase represents a return to "normal" after a cool period at the end of the last century, in which case the average temperature for the eighteenth and nineteenth centuries would have been close to the average for this century.

Comparison of Geothermal and Meteorological Data

Borehole temperature logs can provide information about long-term temperature trends for the period prior to most existing SAT data [*Lachenbruch and Marshall*, 1986; *Lachenbruch et al.*, 1988; *Chapman et al.*, 1992]. A comparison of surface temperature changes inferred alternatively from borehole temperature profiles and from SAT trends for the most recent periods where the signals overlap can also strengthen the confidence in surface ground temperature histories. However surface ground temperature history reconstructions and SAT data are fundamentally different; borehole temperatures are a response to high frequency surface air temperature changes that have been filtered and attenuated in the Earth by the process of heat diffusion.

For our Colorado Plateau data we facilitate the comparison of these two different but complementary data sets by averaging both sets of data thereby providing a view of changing surface temperatures at a regional rather than specific site level. Below 200 m depth the effects of changing surface temperatures should be attenuated and smoothed, but individual reduced temperature plots (Figure 4) show a high-frequency component that cannot be caused by climate change. By stacking these reduced temperatures at their respective depths the effects of random noise are attenuated while the climate signal is retained. The average of reduced borehole temperature data for eight sites (SRS-5 is excluded) is shown in Figure 8a. We have similarly averaged departures from annual mean temperatures observed at the five local weather stations between 1900 and 1990, and passed the average temperature departures through a ten-year Gaussian filter (Figure 8b). This process partially mitigates the effects of data infilling and station relocations. Linear regression analysis of this average air temperature time series yields a temperature increase of 1.3°C over the past 100 years.

The averaged reduced temperatures and averaged SAT time series are now used in two ways. In the first case the SAT data are used as a forcing function at the surface of the Earth and transformed into a synthetic temperature-depth profile. This exercise yields information about the long-term mean surface temperature and shows that reduced temperatures do track variations in SAT data in the recent past. In the second case we solve the inverse borehole temperature problem and compare the resulting surface ground temperature with SAT data. This procedure provides a check on the validity of the inversion results and indicates the nature of climatic histories that can be retrieved from borehole temperature logs.

To use the averaged SAT time series as a forcing function at the surface of the Earth and transform it into a synthetic temperature depth profile, we need to assume a long-term or preobservational mean (POM) [*Lachenbruch et al.*, 1988; *Chisholm and Chapman*, 1992; *Chapman et al.*, 1992]. In practice we find the POM in a forward sense by sweeping through a series of values, accepting the POM that minimizes the rms misfit between the average observed temperatures and the synthetic reduced temperatures calculated from the SAT data (Figure 8a). The best fitting POM is 0.4°C below the 100-year average of the annual mean temperatures. Choices of preobservational mean temperatures near the minimum SATs observed from 1905 to 1930 or near the much higher SATs recorded between 1950 and 1980 provide significantly poorer fits to the reduced temperatures. The best fitting synthetic reduced temperature yielded an rms error of 0.01°C (inset of Figure 8a). There is good correlation between the modeled and observed signals in both amplitude of warming and depth of perturbed temperatures.

As the last step we invert the averaged reduced temperatures for surface ground temperature history and compare it directly to the averaged SAT record (Figure 8b). Analysis of the diagnostic parameters as a function of p (the number of nonzero eigenvalues) indicated a preferred model for $p = 2$. These two steps illustrate dramatically the effects of diffusion, as all high-frequency components of the average SAT signal are missing, both in the synthetic temperature profile (Figure 8a) and the surface ground temperature history (Figure 8b). Nevertheless, we are able to retrieve the long-period temperature signal. Our analysis indicates that the long term mean temperature is 0.4°C below the 1900-1980 average temperature departures derived from the SAT records. Additionally, the Colorado Plateau of eastern Utah has undergone warming of 0.7°C over the past 100 years, and the warming has increased since 1960.

Air and Ground Temperatures

Our analysis suggests that changes in air temperature through time are accompanied by corresponding changes in ground temperatures. However, the SAT at a site may be quite different from its surface ground temperature, even when averaged over several annual cycles. The offset between the two is often difficult to ascertain. Ideally, one would use air temperature measured at a meteorological station and the surface ground temperature inferred from a borehole temperature profile located at the weather station, but these do not exist for southeastern Utah. Instead, we have plotted our borehole surface temperature intercepts (from Table 2) and average air temperature (from Table 3) against elevation of the site or station. Figure 9 demonstrates that the primary difference between values within each data set can be attributed to the lapse rate of decreasing temperature with increasing elevation. For the boreholes the best fitting lapse rate is about -6°C/km; the best fitting lapse rate for the average annual mean air temperatures is about -7°C/km. Due to the small sample size these lapse rates are not statistically different. *Powell et al.* [1988] calculated the lapse rate for a larger area in Utah encompassing many climatic zones using both meteorological and geothermal data and found a lapse rate of -7°C/km. Misfit from the best fitting lapse rate for individual sites and stations suggests that local microclimatological effects are also significant. The average offset between air and ground temperature for southeastern Utah is about 4°C (Figure 9) and is typical of the value determined from a larger data set in Utah [*Powell et al.*, 1988].

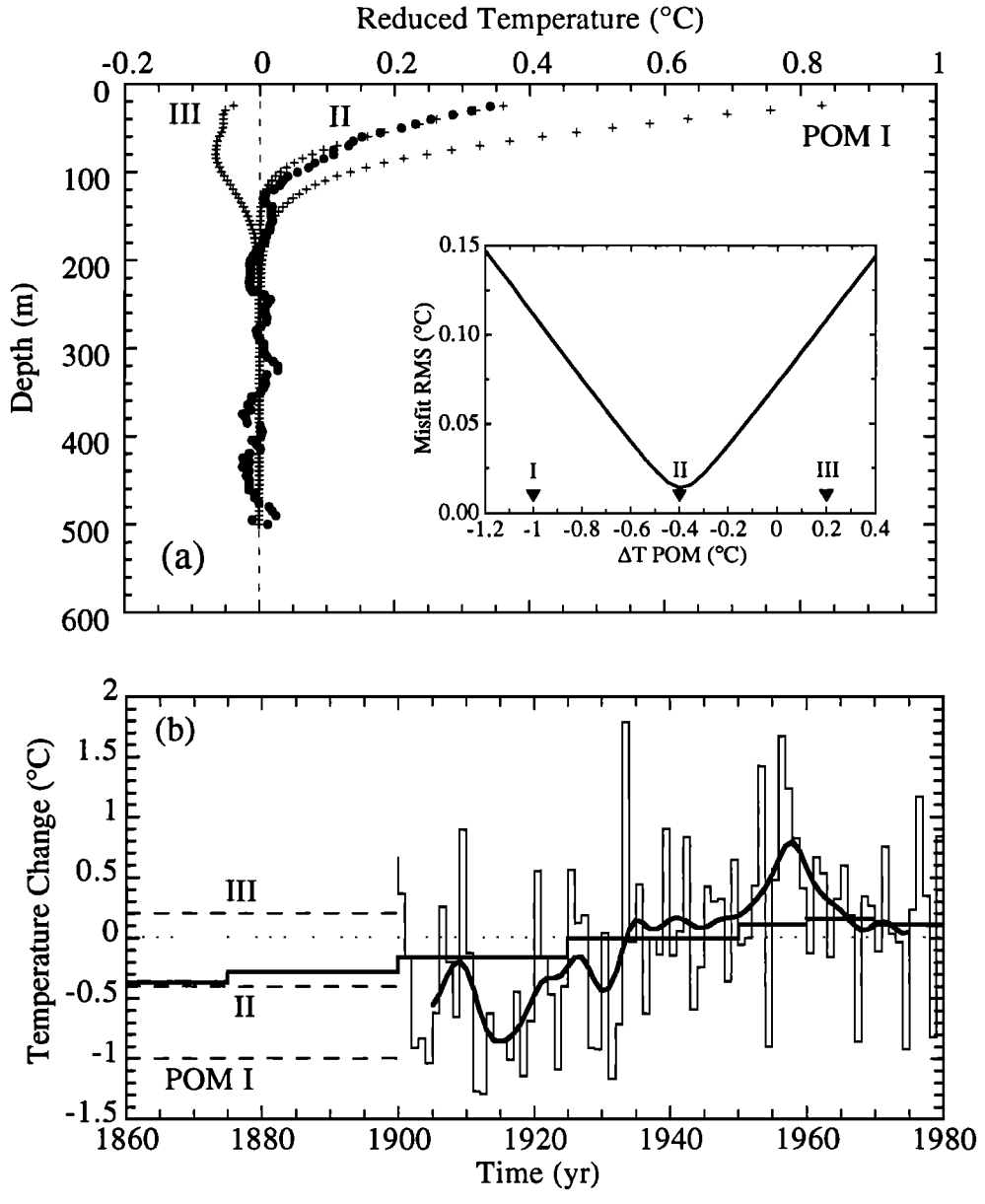

Figure 8. Combining meteorological and geothermal data to infer a ground temperature history. (a) Average reduced temperature profile for all boreholes except SRS-5 (solid circles) compared with synthetic reduced temperature profiles computed from the temperature time series shown in the bottom panel for three choices of a preobservational mean (POM) for time prior to 1900. Inset shows rms misfit as a function of POM and illustrates the best fit of POM II. (b) Surface air temperature record averaged for five weather stations (see Figures 1 and 7) from 1900 to 1980 with three choices of a POM temperature for time prior to 1900. Heavy lines show the average temperature departures passed through a ten-year Gaussian filter (continuously varying curve between 1905 and 1975) and preferred surface ground temperature inversion model for the averaged borehole data corresponding to eigenvalue cutoff $p = 2$ (step-function between 1700 and 1980). For times prior to 1860 the surface ground temperature model is has a value of -0.4°C.

Alternative Explanations

A fundamental assumption in this study has been that departures from linear Bullard plots (i.e., departures from a constant vertical heat flow condition on a plot of temperature versus summed thermal resistance) are transient features and are caused by changes in surface temperature with time. Any errors in that assumption lead directly to errors in reconstructing surface temperature histories and to errors in our conclusions. It is therefore important to examine other processes or disturbances that may produce curvature in a Bullard plot and estimate their magnitudes. Candidate processes and properties include (1) variation of thermal conductivity with depth not considered in our Bullard plot analysis, (2) heat production of rocks, (3) surface elevation effects, (4) lateral variation of surface temperature caused by surface orientation and/or vegetation, (5) uplift and erosion or subsidence and burial at the site, and (6) vertical groundwater flow. These effects and

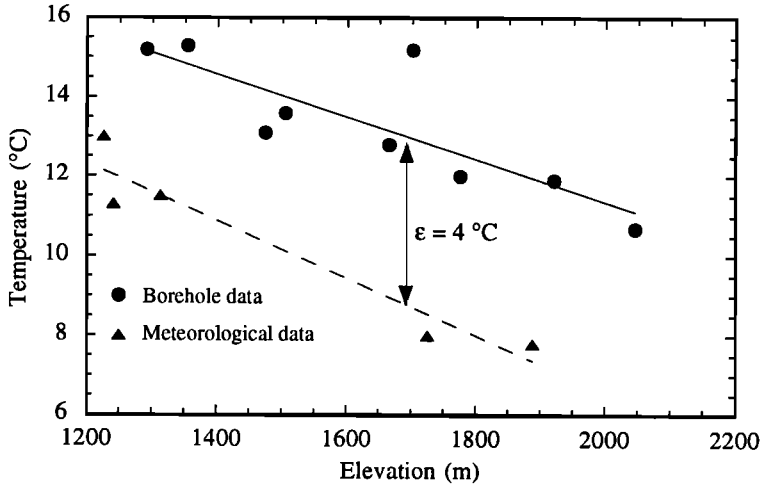

Figure 9. Temperature lapse with elevation for both borehole data (circles) and meteorological data (triangles). Linear regression for borehole and meteorological data are indicated with lines.

their effect on a temperature-depth profile are described in detail in the appendix of *Chisholm and Chapman* [1992].

Thermal conductivity variations are most difficult to dismiss, even though conductivity variation between formations is explicitly included in the analysis. Any spurious effects would have to be caused by lateral and vertical variations in conductivity departing from the values reported in Table 1. Although the Bullard plots (Figure 3) exhibit slight nonlinearity correlated with formations at various depths in each borehole, the major temperature anomalies that we are interpreting for climate change are independent of specific sedimentary formations and are continuous across formation boundaries. As the beds are either horizontal or dip at a shallow angle, refraction of heat caused by lateral conductivity variation is minor. Nevertheless, the following four processes and effects could lead to vertical thermal conductivity variations within formations and thus spurious reduced temperature anomalies: (1) compaction, (2) partial water saturation, (3) lithology/mineralogy change, and (4) thermal conductivity anisotropy.

Compaction of sedimentary rocks with increasing depth leads to an increase in thermal conductivity through porosity reduction. For compacted sandstones and siltstones with porosities about 0.15 and less (see Table 1) a typical porosity reduction over a 200-m depth range (the vertical extent of the reduced temperature anomalies in Figure 4) is less than 0.01, and the resulting conductivity increase is less than 2%. An unnoticed increase in thermal conductivity with depth would produce a decrease in thermal gradient with depth and a negative reduced temperature anomaly. Thus compaction produces an effect that is too small and of the opposite sign to explain our anomalies. A similar argument can be used to dismiss partial groundwater saturation, which would produce low conductivity in unsaturated rock near the surface and higher conductivity in water-saturated rock below the water table.

A regular decrease in thermal conductivity by 10 to 20% over a depth range of 200 m caused by mineralogy changes or changing anisotropy could produce reduced temperature anomalies of the magnitude and shape seen in Figure 4. These conductivity variations, however, would have to exist precisely in the uppermost 200 m of each borehole and not below (i.e., where the reduced temperature anomaly is zero), would have to exist at different stratigraphic levels within the same formation at different sites, and would have to exist in five different formations (Summerville, Curtis, Carmel, Navajo, and Coconino), an unlikely set of conditions.

Heat production in crustal rocks resulting from radioactive decay of U, Th, and K produces a systematic decrease in thermal gradient with depth. However, the departure from a constant temperature gradient is too small to be observed in shallow and intermediate depth boreholes, even for very high values of heat production. A heat production of 1.0 $\mu W\ m^{-3}$, typical of many sedimentary rocks, produces less than 0.04°C reduced temperature anomaly in a 500-m hole. Furthermore, heat production causes a decreasing gradient with increasing depth, just the opposite from an increasing gradient with depth observed at most of our Colorado Plateau sites.

The effect of topography on subsurface temperatures is well known [*Jeffreys*, 1938; *Bullard*, 1939; *Birch*, 1950; *Jaeger*, 1965; *Lachenbruch*, 1969; *Kappelmeyer and Haenel*, 1974; *Powell et al.*, 1988] and amenable to analysis. Isotherms are compressed under valleys, producing locally high thermal gradients, and are separated under hills causing low thermal gradients. The topographically perturbed gradients return to background values at a depth scale equivalent to the wavelength of the topography. Because hills and valleys have a wide range of characteristic dimensions, from tens of meters to kilometers, the subtle effects of topography are potentially dangerous when interpreting departures from constant gradients as transient effects of climate change. Most of our Colorado Plateau sites have planar topography surrounding the sites, in which case the topographic disturbance to the temperature-depth profile is negligible. We have made quantitative estimates of the topographic effect at several sites and find that the curvature in temperature-depth profiles for this topographic effect is close to the noise level in borehole measurements.

In addition to the purely topographic effect discussed above, uneven terrain can produce other subsurface temperature perturbations related to (1) uneven solar radiation received and (2) vegetation differences. The latter are difficult to quantify [*Geiger*, 1965] but, for our semi-arid study area with little vegetation cover, are considered to be negligible. The effects of variable insolation on a planar surface are also negligible.

Erosion or burial of a site over a prolonged period of time constitutes an advection of material and heat toward or away, respectively, from the Earth's surface. If the erosion/burial is sufficiently slow or sufficiently recent, then the temperature-depth profile is largely unaffected; if the erosion/burial is rapid or continues for a long time, then significant curvature can be introduced into the otherwise linear temperature profile. The thermal consequences of erosion/burial have been addressed by *Benfield* [1949] and *Birch* [1950] and are also outlined briefly in standard texts [*Carslaw and Jaeger*, 1959; *Kappelmeyer and Haenel*, 1974]. A useful summary of the appropriate equations to calculate the effects of erosion/burial on temperature and thermal gradient as a function of depth, as well as type curves showing the effects of erosion/burial rate and duration, are given by *Powell et al.* [1988]. All the Colorado Plateau sites investigated in this study are in potential erosional rather than burial settings. Even allowing for a maximum 1 mm/yr erosion rate for 10 m.y., the curvature in the temperature-depth profiles over the depth range 0 to 600 m can be safely ignored in this study. And as with radiogenic heat production, erosion generated curvature in the temperature profiles is in the opposite sense from that observed at our sites.

A final mechanism which may cause curvature in a borehole temperature-depth profile that could be confused with a transient climatic effect is the advection of heat by vertical groundwater flow. Downward migration of water depresses isotherms, creating a concave upward temperature profile similar to that caused by transient warming; upward percolation of warm water creates the opposite effect. Because our Colorado Plateau sites are in relatively permeable sedimentary rock, especially those holes penetrating the Navajo sandstone, this alternative explanation merits rigorous quantitative examination.

We investigate the vertical groundwater flow hypothesis by solving the one-dimensional steady state advection diffusion equation,

$$\frac{\partial^2 T}{\partial z^2} - \frac{\theta \rho_w c_w}{k_e} V_z \frac{\partial T}{\partial z} = 0, \tag{12}$$

where θ is porosity, k_e is effective thermal conductivity, $\rho_w c_w$ is the heat capacity of water, and V_z is the mean vertical velocity. At the surface $T(z = 0) = T_o$, and consistent with our constant heat flow assumption, we use a constant heat flux at a depth L, near the bottom of the perturbed temperatures as the lower boundary condition $\left(\partial T(z)/\partial z\right)_{z=L} = \Gamma_L$. The solution for this model is

$$T(z) = T_o + \frac{\Gamma_L L}{\beta} \frac{\exp\left(\frac{\beta z}{L}\right) - 1}{\exp(\beta)} \tag{13}$$

where

$$\beta = \frac{\theta \rho_w c_w V_z L}{k_e}. \tag{14}$$

the Peclet number.

Mansure and Reiter [1979] show that by integrating (12) once and evaluating the undetermined constant at $z = 0$, where $T = T_o$ and $\left(\partial T(z)/\partial z\right)_{z=0} = \Gamma_o$, yields

$$\frac{\partial T}{\partial z} = \frac{\beta}{L}(T - T_o) + \Gamma_o, \tag{15}$$

where Γ_o is the observed thermal gradient at the surface. This equation permits one to estimate V_z graphically by plotting $\partial T/\partial z$ against $(T-T_o)$ for the thermally perturbed portion of the borehole. Equation (15) shows that the slope of the best fitting line is β/L, and V_z can be estimated from

$$V_z = \frac{\beta}{L} \frac{k_e}{\theta \rho_w c_w}. \tag{16}$$

To estimate groundwater velocity using (15), it is necessary to transform reduced temperatures to temperatures using a background gradient. Because of variations in thermal conductivity, and because the reduced temperatures are averaged with respect to depth, there is no one single thermal conductivity or one thermal gradient associated with each depth. However, the Bullard method indicates an average heat flow of 52 mW m^{-2}, and the conductivity analysis indicates a thermal conductivity with a harmonic mean of about 3.9 W m^{-1} K^{-1}. This gives an estimate of the average background gradient of about 13°C/km. Figure 10 is a $\partial T/\partial z$ versus $(T-T_o)$ plot for the transformed temperature-depth data. This figure shows two zones which can be interpreted in terms of two separate hydrologic regimes. The first region extends to a depth of about 135 m and is characterized with a nonzero slope, possibly caused by vertical water movement. Linear regression over this section of data indicates a slope of 3.9×10^{-3} m^{-1}, which for $\theta = 0.12$, $k_e = 3.9$ W m^{-1} K^{-1}, and $\rho_w c_w = 4186$ J m^{-3} K^{-1} yields a downward vertical groundwater velocity of 1.2 m/yr. The second region is characterized by highly scattered data with no particular trend. Choice of a higher background thermal gradient for this analysis reduces slightly the groundwater velocity needed to produce the observed anomaly but does not change the principal result.

The average annual precipitation in this region, however, is only 0.2 m/yr (U.S. Weather Bureau), and, generally, less than 20% of rainfall infiltrates to the water table. Vertical recharge allowed by meteorological observations is therefore about 0.04 m/yr, clearly inconsistent with a groundwater velocity of 1.2 m/yr inferred from our calculation on the assumption that groundwater flow is responsible for the reduced temperature anomaly. We also note that most of the borehole sites are located at positions in the groundwater flow system midway between the high-elevation recharge areas and discharge regions in low-elevation drainage basins, so that the flow system would be characterized by subhorizontal rather than vertical flow. Finally, it would be highly fortuitous if the vertical groundwater flow at each site ceased at a depth of about 150 m, the depth of significant temperature residuals, because drill logs indicate that the first occurrence of a low-permeability layer has a depth of about 400 m. For these multiple reasons we think it is safe to conclude that the reduced temperature signal in this region cannot be solely due to vertical groundwater flow.

Could part of the reduced temperature signal be caused by vertical groundwater flow? If we assume that the lowest detectable value of $\beta = 0.2$ and that L is about 100 m, then by using (16) the lower limit of detectable curvature has a groundwater velocity is 0.6 m/yr. Thus the average annual precipitation of 0.2 m/yr is not likely to introduce anomalous curvature in temperature-depth measurements.

Conclusions

Temperature profiles from a sequence of boreholes on the Colorado Plateau of southeastern Utah have been examined for evidence of surface warming or cooling that might be

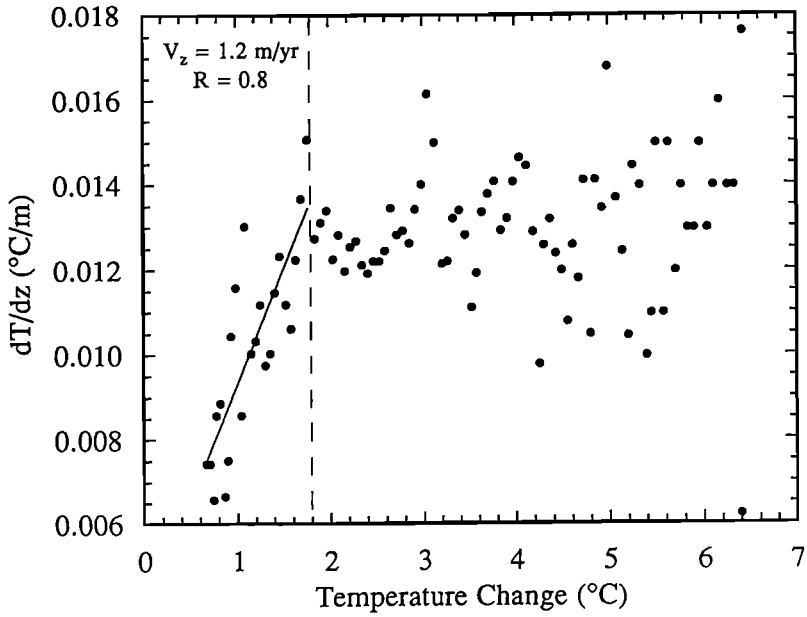

Figure 10. Temperature gradient versus temperature plot for Colorado Plateau averaged reduced temperature profile. The data show two distinct regions. The solid line shown is consistent with a downward vertical groundwater velocity V_z of 1.2 m/yr.

associated with climatic change. Our analysis leads us to the following suggestions and conclusions.

1. It is possible to retrieve ground temperature histories from borehole temperature profiles measured in sedimentary rocks. Variable thermal conductivity of the sedimentary layers requires that reduced temperatures be calculated from Bullard plots for conditions of constant heat flow.

2. Of the nine sites investigated, eight sites yield positive reduced temperature anomalies that indicate surface warming, while one site has a negative reduced temperature anomaly. The anomalies have magnitudes up to 0.5°C and extend to depths between 100 and 200 m.

3. Reduced temperatures were inverted for a surface ground temperature history at each borehole site using a singular value decomposition algorithm. The solution is parameterized in terms of 13 time steps increasing in duration and going back 400 years. Eight of nine borehole sites indicate between 0.4 and 0.8°C (±0.2°C) surface warming over the past 200 years with some evidence for accelerated warming in this century. The aberrant site (SRS-5) indicates two centuries of cooling followed by recent warming, with the present surface temperature still below the long-term mean temperature. These results extend, and are broadly consistent with, the analysis of *Chisholm and Chapman* [1992] showing 0.6°C warming in the northern Basin and Range of Utah.

4. Surface air temperature (SAT) records from five weather stations surrounding the borehole sites all show warming in this century. The magnitude of the SAT trends varies from 0.1 to 2.3°C/century with an average of 1.3°C/century. A synthetic reduced temperature-depth profile computed by using the average SAT time series as a forcing function provides an excellent match to the regionally averaged borehole temperature anomaly but only for a restricted choice of preobservational mean temperature. The best fitting POM is 0.4°C below the 80-year average of the annual mean temperatures.

5. Nonclimatic explanations for the borehole temperature anomalies, including slow vertical infiltration of groundwater through the sedimentary rocks, were considered but found lacking.

Acknowledgments. We appreciate thoughtful reviews from H. Beltrami, D. Issler, and J. Majorowicz. This paper also benefited from comments by T. Chisholm, D. Deming, R. Saltus, and K. Wang. This research was supported by NSF grants EAR-9104292 and EAR-9205031.

References

Beck, A. E., Precision logging of temperature gradients and the extraction of past climate, *Tectonophysics, 83*, 1–11, 1982.

Beltrami, H., and J. C. Mareschal, Recent warming in eastern Canada inferred from geothermal measurements, *Geophys. Res. Lett., 18*, 605–608, 1991.

Beltrami, H., and J. C. Mareschal, Ground temperature histories for central and eastern Canada from geothermal measurements: Little Ice Age signature, *Geophys. Res. Lett., 19*, 689–692, 1992.

Beltrami, H., and J. C. Mareschal, Resolution of ground temperature histories inverted from borehole temperature data, *Global Planet. Change*, in press, 1994.

Benfield, A. E., The effect of uplift and denudation on underground temperatures, *J. Appl. Phys., 20*, 66–70, 1949.

Birch, F., The effects of Pleistocene climatic variations upon geothermal gradients, *Am. J. Sci.*, 246, 729–760, 1948.

Birch, F., Flow of heat in the Front Range, Colorado, *Geol. Soc. Am. Bull., 61*, 567–620, 1950.

Bodell, J. M., and D. S. Chapman, Heat flow in the north-central Colorado Plateau, *J. Geophys. Res., 87*, 2869–2884, 1982.

Briffa, K. R., and P. D. Jones, Global surface air temperature variations during the twentieth century, Part 2, Implications for large-scale high-frequency palaeoclimatic studies, *Holocene, 2*, 77–88, 1993.

Bullard, E. C., Heat flow in South Africa, *Proc. R. Soc. London* Series *A, 173*, 474–502, 1939.

Carslaw, H. S., and J. C. Jaeger,*Conduction of Heat in Solids*, 386 pp., Oxford University Press, New York, 1959.

Chapman, D. S., Heat flow and heat production in Zambia, Ph.D. thesis, 94 pp., Univ. of Mich., Ann Arbor, 1976.

Chapman, D. S., M. D. Clement, and C. W. Mase, Thermal regime of the Escalante Desert, Utah, with an analysis of the Newcastle geothermal system, *J. Geophys. Res., 86*, 11,735–11,746, 1981.

Chapman, D. S., T. J. Chisholm, and R. N. Harris, Combining borehole temperature and meteorologic data to constrain past climate change, *Palaeogeogr. Palaeoclimatol. Palaeoecol., 98*, 269–281, 1992.

Chisholm, T. J., and D. S. Chapman, Climate change inferred from borehole temperatures: An example from western Utah, *J. Geophys. Res., 97*, 14,155–14,176, 1992.

Clow, G. D., The extent of temporal smearing in surface-temperature histories derived from borehole temperature measurements, *Palaeogeogr. Palaeoclimatol. Palaeoecol., 98*, 81–86, 1992.

Deming, D., and R. Borel, Evidence for possible climate change in the southern plains province of the U.S. for borehole temperature profiles, *EosTrans. AGU, 74*, (43), Fall Meeting suppl., 607, 1993.

Ellsaesser, H. W., M. C. MacCracken, J. J. Walton, and S. L. Grotch, Global climatic trends as revealed by the recorded data, *Rev. Geophys., 24*, 745–792, 1986.

Geiger, R., *The Climate Near the Ground*, 611 pp., Harvard University Press, Cambridge, Mass., 1965.

Gosnold, W. D., Jr., and M. Bauer, The climate record in borehole temperatures in the north central United States, (abstract) *Eos Trans. AGU, 71*, 1597, 1990.

Hansen, J., and S. Lebedeff, Global trends of measured surface air temperature, *J. Geophys. Res., 92*, 13,345–13,372, 1987.

Jackson, D. D., Interpretation of inaccurate, insufficient and inconsistent data, *Geophys. J. R. Astr. Soc., 28*, 97–109, 1972.

Jaegar, J. C., Application of the theory of heat conduction to geothermal measurements, in *Terrestrial Heat Flow*, Geophys. Monogr. Ser., vol. 8, pp. 7–23, edited by W. H. K. Lee, *AGU*, D. C., 1965.

Jeffreys, H., The disturbance of the temperature gradient in the Earth's crust by inequalities of height, *Mon. Not. R. Astron. Soc., Geophys. Suppl., 4*, 309–312, 1938.

Jessop, A., Geothermal evidence of climate change, *Eos Trans. AGU, 71*, 385–399, 1990.

Jones, P. D., and K. R. Briffa, Global surface air temperature variations during the twentieth century, Part 1, Spatial, temporal and seasonal details, *Holocene, 2*, 165–179, 1992.

Kappelmeyer, O., and R. Haenel, *Geothermics, With Special Reference to Application*, 238 pp., Gebruder Borntraeger, Berlin, 1974.

Lachenbruch, A. H., The effect of two dimensional topography on superficial thermal gradients, *U.S. Geol. Surv. Bull., 1203–E*, 86 pp., 1969.

Lachenbruch, A. H., and B. V. Marshall, Changing climate: Geothermal evidence from permafrost in the Alaskan Arctic, *Science, 234*, 689–696, 1986.

Lachenbruch, A. H., T. T. Cladouhos, and R. W. Saltus, Permafrost temperature and the changing climate, paper presented at 5th International Conference on Permafrost, Trondheim, Norway, Aug. 1988.

Lanczos, C., *Linear Differential Operators*, pp. 124–127, D. Van Nostrand, Princeton, N. J., 1961.

Lines, L. R., and S. Treitel, A review of least squares inversion and its application to geophysical problems, *Geophys. Prospect., 32*, 159–186, 1984.

Mansure, A. J., and M. Reiter, A vertical groundwater movement correction for heat flow, *J Geophys. Res., 84*, 3490–3496, 1979.

Mareschal J. C., and H. Beltrami, Evidence for recent warming from perturbed geothermal gradients: examples from eastern Canada, *Clim. Dyn., 6*, 135–143, 1992.

Mareschal, J. C., and G. Vasseur, Ground temperature history from two deep boreholes in central France, *Palaeogeogr. Palaeoclimatol. Palaeoecol., 98*, 185–192, 1992.

Nielsen, S. B., and A. E. Beck, Heat flow density values and paleoclimate determined from stochastic inversion of four temperature-depth profiles from the Superior Province of the Canadian Shield, *Tectonophysics, 164*, 345–359, 1989.

Phillips, R. J., Techniques in Doppler gravity inversion, *J. Geophys. Res., 79*, 2027–2036, 1974.

Powell, W. G., D. S. Chapman, N. Balling, and A. E. Beck, Continental heat flow density, in *Handbook of Terrestrial Heat-Flow Density Determinations*, edited by R. Haenel, L. Rybach, and L. Stegena, pp. 167–222, Kluwer Academic, Boston, Mass., 1988.

Somerton, W. H., *Thermal Properites and Temperature-Related Behavior of Rock/Fluid Systems*, 257 pp., Elsevier, New York, 1992.

Wang, K., and T. J. Lewis, Geothermal evidence from Canada for a cold period before recent climatic warming, *Science, 256*, 1003–1005, 1992.

Wigley, T. M. L., J. Angell, and P. D. Jones, Analysis of the temperature record, in Detecting the Climatic Effects of Increasing Carbon Dioxide, Rep. *DOE/ER–0235*, 198 pp., Dep. of Energy, Washington, D. C., 1985.

D. S. Chapman and R. N. Harris, Department of Geology and Geophysics, 717 W. C. Browning Building, University of Utah, Salt Lake City, UT 84112-1183. (e-mail: rnharris@mines.utah.edu)

(Received April 19, 1994; revised August 11, 1994; accepted August 15, 1994.)